APL Materials

RESEARCH ARTICLE | JUNE 01 2023

Probing the energy levels of organic bulk heterojunctions by varying the donor content

Special Collection: **Advances in Organic Solar Cells**

Anna Jungbluth ; Pascal Kaienburg ; Andreas E. Lauritzen ; Thomas Derrien ; Moritz Riede

Check for updates

APL Mater 11, 061105 (2023)
https://doi.org/10.1063/5.0148191

CrossMark
View Online
Export Citation

09 August 2023 09:53:30

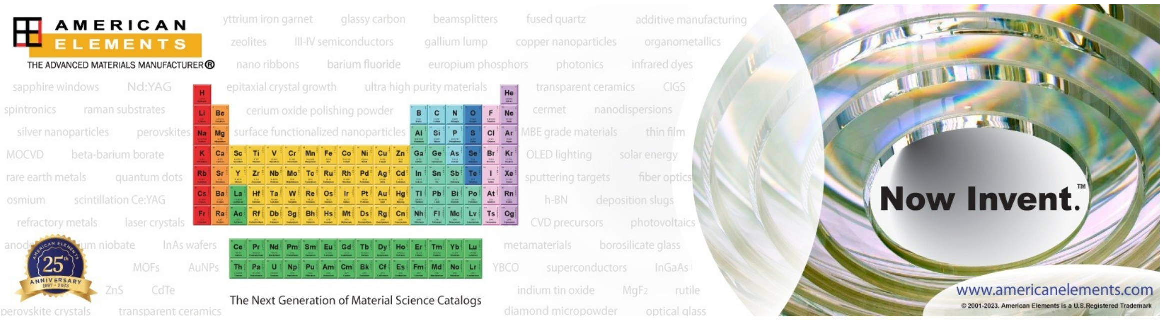
AMERICAN ELEMENTS
THE ADVANCED MATERIALS MANUFACTURER®
yttrium iron garnet glassy carbon beamsplitters fused quartz additive manufacturing
zeolites III-IV semiconductors gallium lump copper nanoparticles organometallics
nano ribbons barium fluoride europium phosphors photonics infrared dyes
sapphire windows Nd:YAG epitaxial crystal growth ultra high purity materials transparent ceramics CIGS
spintronics raman substrates cerium oxide polishing powder cermet nanodispersions
silver nanoparticles perovskites surface functionalized nanoparticles MBE grade materials thin film
MOCVD beta-barium borate OLED lighting solar energy
rare earth metals quantum dots sputtering targets fiber optics
osmium scintillation Ce:YAG h-BN deposition slugs
refractory metals laser crystals CVD precursors photovoltaics
InAs wafers metamaterials borosilicate glass
MOFs AuNPs YBCO superconductors InGaAs
ZnS CdTe indium tin oxide MgF2 rutile
perovskite crystals transparent ceramics diamond micropowder optical glass
The Next Generation of Material Science Catalogs
Now Invent.™
www.americanelements.com
© 2001-2023. American Elements is a U.S. Registered Trademark

AIP Publishing

APL Materials ARTICLE scitation.org/journal/apm

Probing the energy levels of organic bulk heterojunctions by varying the donor content

Cite as: APL Mater. 11, 061105 (2023); doi: 10.1063/5.0148191
Submitted: 28 February 2023 • Accepted: 28 April 2023 •
Published Online: 1 June 2023

Anna Jungbluth,[1] **Pascal Kaienburg,**[1] **Andreas E. Lauritzen,**[1] **Thomas Derrien,**[2,a)] **and Moritz Riede**[1,b)]

AFFILIATIONS

[1] Department of Physics, The University of Oxford, Oxford, Oxfordshire OX13PU, United Kingdom
[2] Diamond Light Source, Didcot, Oxfordshire OX11 0DE, United Kingdom

Note: This paper is part of the Special Topic on Advances in Organic Solar Cells.
[a)] **Current address:** Living Systems Institute, University of Exeter, Exeter EX4 4QD, United Kingdom.
[b)] **Author to whom correspondence should be addressed:** moritz.riede@physics.ox.ac.uk

ABSTRACT

The performance of organic solar cells is strongly governed by the properties of the photovoltaic active layer. In particular, the energetics at the donor (D)–acceptor (A) interface dictate the properties of charge transfer (CT) states and limit the open-circuit voltage. More generally, energetic landscapes in thin films are affected by intermolecular, e.g., van der Waals, dipole, and quadrupole, interactions that vary with D:A mixing ratio and impact energy levels of free charges (ionization energy, electron affinity) and excitons (singlet, CT states). Disentangling how different intermolecular interactions impact energy levels and support or hinder free charge generation is still a major challenge. In this work, we investigate interface energetics of bulk heterojunctions via sensitive external quantum efficiency measurements and by varying the D:A mixing ratios of ZnPc or its fluorinated derivatives and C_{60}. With increasing donor fluorination, the energetic offset between F_xZnPc and C_{60} reduces. Moving from large to low offset systems, we find qualitatively different trends in device performances with D:C_{60} mixing ratios. We rationalize the performance trends via changes in the energy levels that govern exciton separation and voltage losses. We do so by carefully analyzing shifts and broadening sEQE spectra on a linear and logarithmic scale. Linking this analysis with molecular properties and device performance, we comment on the impact of charge–quadrupole interactions for CT dissociation and free charge generation in our D:C_{60} blends. With this, our work (1) demonstrates how relatively accessible characterization techniques can be used to probe energy levels and (2) addresses ongoing discussions on future molecular design and optimal D–A pairing for efficient CT formation and dissociation.

I. INTRODUCTION

The performance of organic solar cells (OSCs) is dependent on, for instance, molecular design, device architectures, and fabrication conditions, offering a large parameter space to explore and optimize. Compared to other solar cell technologies, e.g., perovskites, which are mainly limited by charge carrier recombination between material layers,[1] OSCs are currently mainly limited by large energy losses in the bulk of the photovoltaic active layer and specifically at donor (D)–acceptor (A) interfaces. While bulk energy levels influence exciton diffusion and charge transport,[2] the energetics at the D–A interface impact the properties of charge transfer (CT) states[3] and determine the efficiency of (1) charge transfer from singlet (S_1) to CT states, (2) exciton dissociation from CT to charge separated (CS) states, and (3) recombination to the ground state (GS). Therefore, studying and optimizing energetic landscapes and transitions, especially of excited S_1 and CT states in D–A blends, is crucial for increasing photocurrents and reducing recombination losses of OSCs. Nonetheless, an accurate determination of molecular and blend energy levels, in particular, around buried D–A interfaces in bulk heterojunctions (BHJs), remains a challenge.[4] In the context of molecular energy levels, the ionization energies (IE) and electron affinities (EA) of molecules are often used as zeroth order approximations to judge the photovoltaic potential of different D–A pairs[5] and are generally determined via density functional theory (DFT),[4,6] cyclic voltammetry (CV),[7] ultraviolet photoelectron spectroscopy (UPS),[8,9] and inverse photoemission spectroscopy (IPES) on single component films.[6] While these specialized techniques are not always accessible to researchers, the different measurements are rarely comparable[4] and are not directly device relevant if energy levels are probed for isolated molecules, molecules in solution, or thin films grown on specialized substrates rather than full device stacks. In addition, many of these experimental techniques are surface-sensitive and cannot directly probe the bulk. However, studying the energetics of BHJs in device-relevant configurations is paramount to ensure consistency with device characterization techniques. This is because energy levels are strongly impacted by intermolecular interactions (Fig. 1), e.g., polarization effects that reduce the IE–EA gap in thin films compared to isolated molecules, or electrostatic interactions (e.g., van der Waals forces, dipole or quadrupole moments[8,10–13]), that change with D:A mixing ratios, molecular orientation, dielectric constants, and microstructure.[9,14–18] In this context, especially charge–quadrupole interactions have gained significant interest, as they were shown to cause large electrostatic shifts in crystalline[10,11,13,19] and disordered organic films.[8,20,21] More specifically, a molecule with a non-zero quadrupole moment creates an electrostatic field that causes the energy levels of molecules in its vicinity to shift. The resulting change in IE and EA occurs in the same direction and by roughly the same amount. While the direction of the energetic shift depends on the sign of the quadrupole,[8] the magnitude depends on the strength of the electrostatic field and hence the magnitude of an individual quadrupole, the number of quadrupoles, and the distance between the quadrupole and surrounding molecules.[20] With this, the precise effect of charge–quadrupole interactions on the energy levels in BHJs is dependent on the quadrupole moments of the chosen donor/acceptor molecules and D–A mixing and is generally different in the bulk than at the interface [Figs. 1(b) and 1(c)].[8] As a result, specifically, an exciton dissociation from CT to CS states is strongly influenced by charge–quadrupole effects[8] and either supported or hindered depending on the precise molecular interactions.

In this work, we investigate the role of D:A mixing on the energetic landscape of BHJ devices based on zinc phthalocyanine (ZnPc) or its fluorinated derivatives (F_4ZnPc, F_8ZnPc, and F_{16}ZnPc) as donors and C_{60} as the acceptor [Fig. 2(a) and Fig. S1]. Fluorination of ZnPc molecules simultaneously shifts the IE and EA away from the vacuum level,[22,23] thereby increasing the interfacial CT state energy (and decreasing $\Delta E_{CT} = E_{S_1} - E_{CT}$, the driving force for CT) in blends with C_{60}. Gradual fluorination of ZnPc also increases the molecular quadrupole moments,[8,20] resulting in stepwise changes in the electrostatic environment. In the F_xZnPc:C_{60} blends, the donor molecules have considerable quadrupole moments [Fig. 2(a)] while the quadrupole moment of C_{60} is zero. Consequently, the energy level shifts of F_xZnPc molecules in thin film blends are expected to directly increase with donor content and are larger in pure donor phases than at the interface with C_{60}.[8] Similarly, C_{60} energy level shifts are smaller (or even zero) in pure phases of C_{60} compared to the D–A interface. For each donor molecule, we systematically vary the donor content from neat C_{60} to neat F_xZnPc (x = 0, 4, 8, and 16) and study device performances via current density–voltage (J–V) measurements. We use sensitive external quantum efficiency (sEQE) measurements as a relatively accessible technique to study energy levels in full device stacks.[24,25] This is done by fitting the energy of singlet (E_{S_1}) and CT states (E_{CT})—the most device relevant energy levels—from sEQE spectra using Marcus theory.[26–31] We find that device performances are strongly dependent on D:C_{60} mixing ratios for all materials, with ZnPc:C_{60}/F_4ZnPc:C_{60} and F_8ZnPc:C_{60}/F_{16}ZnPc:C_{60} displaying similar performance trends.[32] Compared to our previous work, where we studied charge transfer and charge separation in low donor content blends (D:A [5:95]) of F_xZnPc and C_{60},[32] this work explores how donor content impacts energy levels and device performance. This is especially interesting considering that aggregation-induced

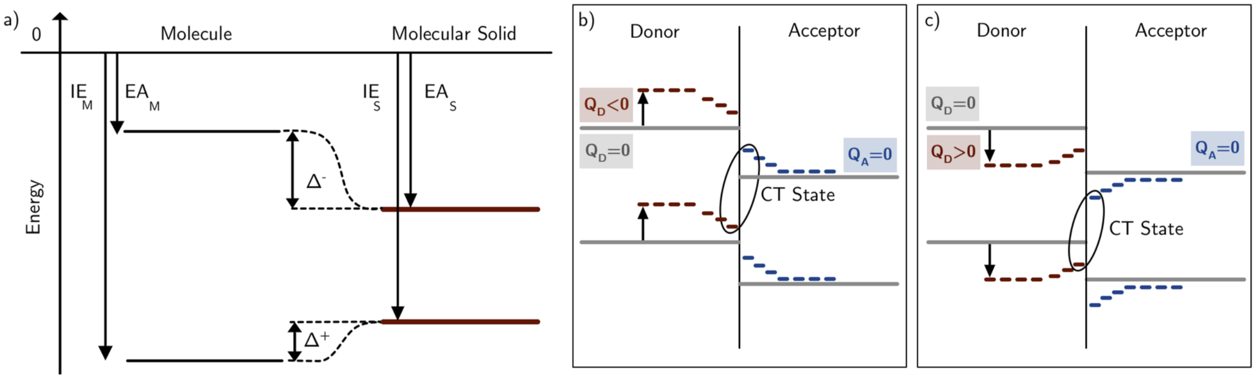

FIG. 1. (a) Schematic energy level changes from isolated molecules (M) to molecular solids (S) and [(b) and (c)] energy levels at the donor–acceptor heterojunction. Intermolecular interactions (Δ^+, Δ^-) decrease the energetic difference between the ionization energy (IE) and electron affinity (EA) in molecular solids compared to isolated molecules. These interactions encompass both polarization (i.e., via the distortion of charge distributions)[57] and electrostatic effects (e.g., via charge, dipole, or quadrupole interactions).[8,10,13] While polarization effects move the IE and EA closer together, charge–quadrupole interactions shift the IE and EA by the same amount and in the same direction [schematics (b) and (c)]. Depending on the sign of the quadrupole moment (Q) of the donor (D) or acceptor (A) molecules, the IE/EA shift (b) toward or (c) away from the vacuum level.[8] The gray solid lines show the hypothetical energy levels if $Q_D = 0$. The energy level shifts depend on the strength of the electrostatic field, i.e., on the magnitude of the quadruple moments and the number of quadrupoles present. The schematics were adapted from references.[8,51,58,59]

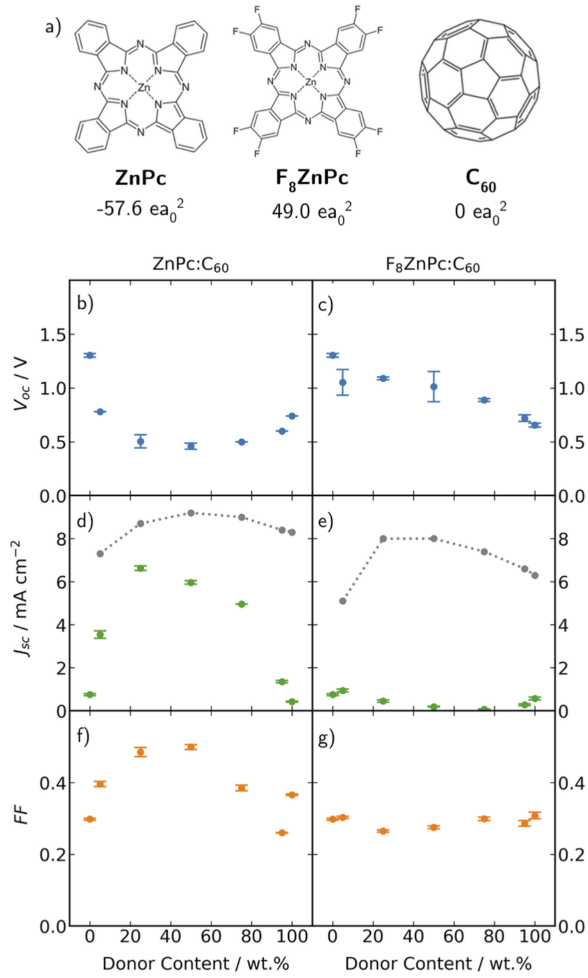

FIG. 2. (a) Molecular structure and quadrupole moments in the π–π stacking direction of (b)–(g) V_{oc} (top row), J_{sc} (middle row), and *FF* (bottom row) as a function of donor fluorination and D:C$_{60}$ mixing ratio for ZnPc [(b), (d), and (f)] and F$_8$ZnPc [(c), (e), and (g)] blends with C$_{60}$. All measurements were performed under simulated 1 Sun illumination with respect to a silicon reference diode and at room temperature. The data are plotted as measured and are included in Table S2. Spectral mismatch correction of our samples only marginally shifts the J_{sc} and preserves all observed performance trends (see Fig. S5). The gray dotted data points (middle row) were simulated via transfer matrix modeling of the J_{sc}, assuming that all absorbed photons in the D:A layer lead to free charge carriers and that charge collection is ideal (IQE = 100%).

polarization effects and charge–quadrupole interactions are absent at low donor content when donor aggregation is suppressed.[33–35] In agreement with recent research,[8] we find an empirical correlation between the sign of the donor quadrupole moment ($Q_D \neq 0$; $Q_{C_{60}} = 0$) and whether photocurrents increase or decrease with donor content. While D:A mixing series are often only used to optimize device performances, our work demonstrates that simple analyses of sEQE spectra can provide valuable insights on the energy levels of D:A blends and help uncover the underlying principles governing device performance.

II. THE IMPACT OF DONOR FLUORINATION AND DONOR CONTENT ON DEVICE PERFORMANCE

We fabricated BHJ devices of F$_x$ZnPc (x = 0, 4, 8, 16) and C$_{60}$ at 0, 5, 25, 50, 75, 95, and 100 wt. % donor content. All samples were fabricated via vacuum thermal evaporation, co-depositing donor, and acceptor molecules in the desired weight ratio. For comparability with other literature reports, Table S1 in the supplementary material summarizes the conversion of donor wt. % to the commonly used mol. % or vol. %. Apart from the active layer, all samples were fabricated with nominally identical device architectures and through subsequent evaporation of MoOx (3 nm, 0.05–0.1 Å/s), F$_x$ZnPc:C$_{60}$ (50 nm, combined rate of 0.4 Å/s), BPhen (8 nm, 0.1–0.2 Å/s), and Al (100 nm, 1–2 Å/s). The substrates were held at room temperature during deposition, and all devices were encapsulated with a glass cover slide in inert conditions prior to measurement.

J–V measurements (Fig. S3 in the supplementary material) of the best performing (highest PCE) devices and sEQE measurements on a linear scale [Figs. 3(a)–3(c) and Figs. S6(a) and S6(c)] reveal that while devices based on neat C$_{60}$ show a high open-circuit voltage (V_{oc}), active layer absorbance is limited and charge separation is poor, leading to a low short-circuit current density (J_{sc}). Adding even small amounts of ZnPc drastically improves the photocurrent [Fig. S3(a)] due to improved charge separation at the D:C$_{60}$ interface.[24,25,36] The same increase in J_{sc} is observed for F$_4$ZnPc [Fig. S3(b)]. While the J_{sc} of the F$_4$ZnPc blends is comparable to the ZnPc blends, the V_{oc} is generally 0.1–0.2 V larger due to the fluorination-induced shift of the donor energy levels that reduce the interfacial energetic offset with C$_{60}$.[8,22,23] Compared to ZnPc and F$_4$ZnPc, the photocurrents of all F$_8$ZnPc [Fig. S3(c)] and F$_{16}$ZnPc [Fig. S3(d)] blends are smaller than for the neat materials, indicating that free charge generation at the D:C$_{60}$ interface is inefficient. Due to the similarities in device performance trends of the ZnPc/F$_4$ZnPc and F$_8$ZnPc/F$_{16}$ZnPc blends, we focus our subsequent discussion on comparing ZnPc:C$_{60}$ and F$_8$ZnPc:C$_{60}$ as representative examples. Device characterization of all F$_x$ZnPc:C$_{60}$ blends is included in the supplementary material for completeness. Figure 2 (and Fig. S4) summarizes the trends in V_{oc}, J_{sc}, and fill factor (*FF*) across donor molecules and donor content. The V_{oc} of the ZnPc series is strongly dependent on D:C$_{60}$ mixing and first decreases for intermixed ZnPc:C$_{60}$ (D:A [50:50]), and then increases with higher ZnPc content [Fig. 2(b)]. This is in agreement with previous reports[9,37] and is attributed to changing E_{CT} (discussed again later) and increasing non-radiative losses for the intermixed blends [Figs. S12(a) and S12(b)]. In comparison, the V_{oc} of the F$_8$ZnPc blends [Fig. 2(c)] decreases from 1.05 ± 0.12 V (low donor content) to 0.66 ± 0.02 V (neat F$_8$ZnPc). This decrease is coupled with a strong increase in non-radiative recombination from ~0.2 to ~0.5 eV [Figs. S12(e) and S12(f)]. The J_{sc} [Fig. 2(d)] and *FF* [Fig. 2(e)] of the ZnPc blends both peaks for intermixed ZnPc:C$_{60}$. The F$_4$ZnPc system (Fig. S4, second column) follows the same trends as ZnPc, although the change in V_{oc} is less pronounced. In comparison, the J_{sc} of F$_8$ZnPc [Fig. 2(e)] shows the opposite trend and decreases for intermixed F$_8$ZnPc:C$_{60}$, while the *FF* stays roughly constant (~0.3). The same is observed for F$_{16}$ZnPc [Figs. S4(d), S4(h), and S4(l)]. Rationalizing these performance trends, especially the increased (decreased) photocurrents for intermixed

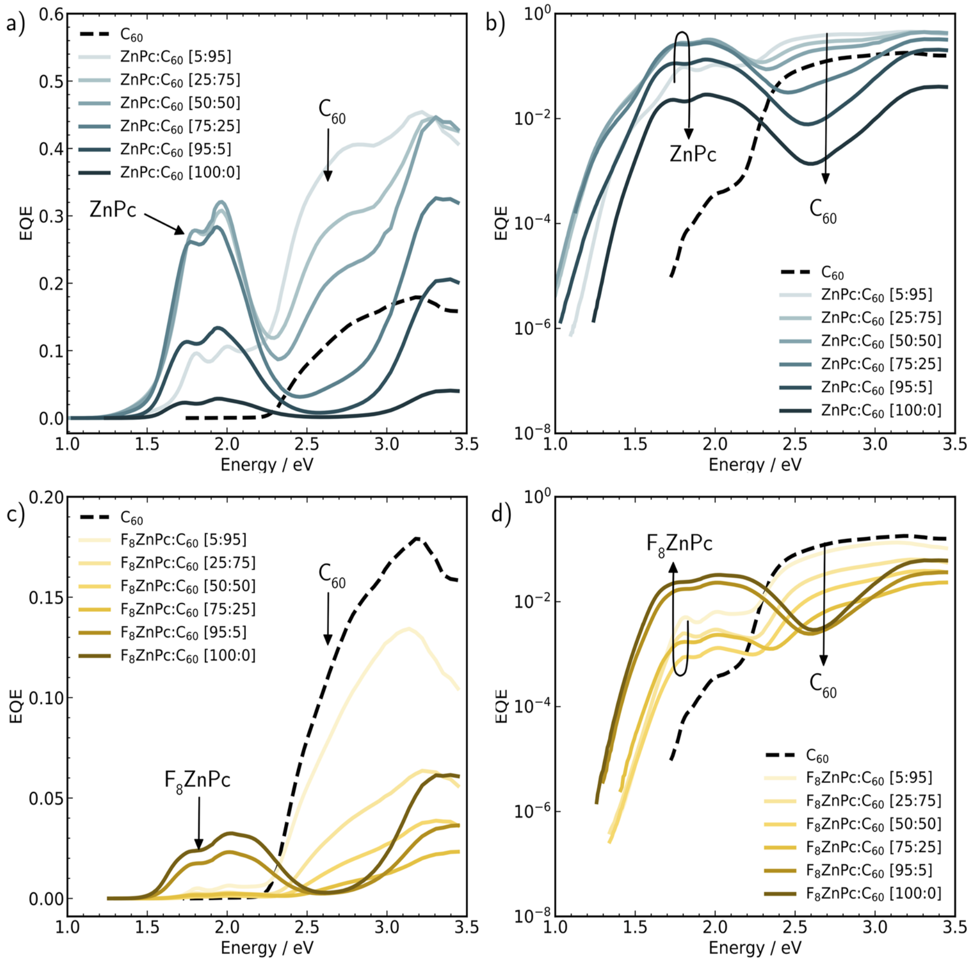

FIG. 3. EQE on a linear (first column) and logarithmic (second column) scale for [(a)–(b)] ZnPc and [(c)–(d)] F_8ZnPc blends with C_{60}. Only the ZnPc:C_{60} blends show a distinguishable CT state peak. Spectral regions where primarily F_xZnPc or C_{60} absorb are highlighted, and the arrows in [(b) and (d)] mark the trends in peak intensity with increasing donor content.

ZnPc:C_{60}/F_4ZnPc:C_{60} (F_8ZnPc:C_{60}/F_{16}ZnPc:C_{60}), we consider that the J_{sc} is strongly dependent on active layer absorbance, charge separation, and charge carrier collection. While this work focuses on interface-related processes of free charge generation and recombination, the microstructure of the blends and implications for charge transport are briefly discussed. Through grazing incidence wide-angle x-ray scattering (GIWAXS) measurements (Fig. S13 in the supplementary material), we find that the microstructure at specific D:C_{60} mixing ratios is largely comparable for all donor molecules. Comparing the different D:A mixing ratios, neat F_xZnPc films show preferential ordering of the molecules in the π–π stacking direction and peak broadening along the azimuthal angle, indicating a large spread in the orientation of individual crystalline domains.[32,38] The low acceptor content blends show weaker F_xZnPc scattering features but an equal spread in the orientation of the F_xZnPc domains (Fig. S13, second column). In comparison, the low donor content blends show no scattering features, indicating that even small amounts of the donor molecules effectively disrupt C_{60} packing (Fig. S13, first column). From our GIWAXS measurements and literature reports of intermixed ZnPc:C_{60},[39] the morphology of our blends can be pictured with some degree of donor/acceptor aggregation at high enough molecular concentrations but no clear phase separation. Phase separation is only clearly observed for samples that are heated during deposition,[40–42] compared to the room temperature substrates used in this study. In terms of percolation, we note that the low donor (acceptor) content blends still achieve charge transport to the electrode, even in the absence of bi-continuous percolation pathways, through mechanisms like long-range tunneling.[35,43] In summary, while the trends in J_{sc} and FF are certainly the result of superimposed effects, the qualitative trends between ZnPc and F_8ZnPc cannot be explained via differences in the microstructure and charge transport. Based on the strong similarities in the donor absorption profiles,[32] absorption changes can also not explain the trends in photocurrent. This is confirmed by transfer matrix modeling (TMM) of the J_{sc} of the ZnPc [Fig. 2(d)] and F_8ZnPc [Fig. 2(e)] blends, which predicts equally high (6–10 mA/cm^2) photocurrents for both donors that peak for 25–50 wt. % donor loading. While the measured photocurrents of the ZnPc blends largely agree with the simulations, aside from the lower J_{sc} for the low donor and low acceptor content blends, F_8ZnPc not only shows severely reduced photocurrents ($\sim 0.5 - 1$ mA/cm^2) but also displays the opposite trend predicted by TMM. This is likely caused by inefficient charge separation in the F_8ZnPc and F_{16}ZnPc blends. Although an in-depth discussion of exciton separation efficiencies is beyond the scope of this study, we note that charge separation occurs after exciton transfer from S_1 to CT states and relies on efficient exciton dissociation from CT to CS states. Especially, the latter is strongly influenced by electrostatic shifts, e.g., caused by charge–quadrupole interactions.[8,20] In blends with C_{60}, the energetic barrier for exciton dissociation ($\Delta E_{diss} = E_{CT} - E_{CS}$) was previously found to decrease for donor molecules with negative quadrupole moments (e.g., ZnPc and F_4ZnPc), thereby assisting free charge generation, while positive quadrupole moments (e.g., F_8ZnPc and F_{16}ZnPc) increase ΔE_{diss}.[8,20] Since charge–quadrupole effects are dependent on film composition and scale with molecular blending,[8,20] they could help rationalize the low photocurrents of the intermixed F_8ZnPc:C_{60} and F_{16}ZnPc:C_{60} blends, which is again discussed later. We next turn to investigate the energetics of S_1 and CT states in our blends to further rationalize device performances.

III. INVESTIGATING ENERGY LEVELS VIA SENSITIVE EXTERNAL QUANTUM EFFICIENCY MEASUREMENTS

S_1 and CT state energies provide invaluable information on molecular and blend energetics in full device stacks with complex intermolecular interactions. Figures 3(b) and 3(d) [and Figs. S6(b) and S6(d)] show sEQE spectra of the investigated systems on a logarithmic scale. Only the ZnPc blends show clearly discernible CT state shoulders. From the sEQE spectra, we also confirm that the S_1 of the donor is lower in energy than that of C_{60}, thereby defining the optical gap of the BHJ blends. To determine the donor E_{S1} and E_{CT}, we follow the approach presented in Refs. 44–46 and fit both the S_1 peaks and CT states in sEQE spectra via Gaussian functions. While S_1 absorption is influenced by homogeneous and inhomogeneous broadening, which leads to an overall Gaussian line shape, charge transfer reactions, such as exciton transfer from S_1 to CT states, are well described by Gaussian functions like Marcus theory.[26–28,30,31] Fitting both S_1 and CT states is more robust than simple fitting of only CT states, especially for systems with low $\Delta E_{CT} = E_{S_1} - E_{CT}$, where CT states are not easily distinguishable.[44] We note that the S_1 peak of C_{60} is hidden in the spectra and cannot easily be fit using the same approach. Figures 4(a) and 4(c) show two example fits for intermixed ZnPc:C_{60} and F_8ZnPc:C_{60}. For completeness, we also plot the sum of the S_1 and CT state fits, which describe the sEQE tail well in both cases. Figures 4(b) and 4(d) (Figs. S8–S10) summarize the fit results for the ZnPc:C_{60} and F_8ZnPc:C_{60} (F_4ZnPc:C_{60} and F_{16}ZnPc:C_{60}) blends as a function of donor content. For blends based on ZnPc, both E_{S_1} and E_{CT} follow the same U-shaped trend as the V_{oc}, resulting in a roughly constant $\Delta E_{CT} \approx 0.3$ eV across ZnPc:C_{60} mixing ratios (Table S4). Previous work

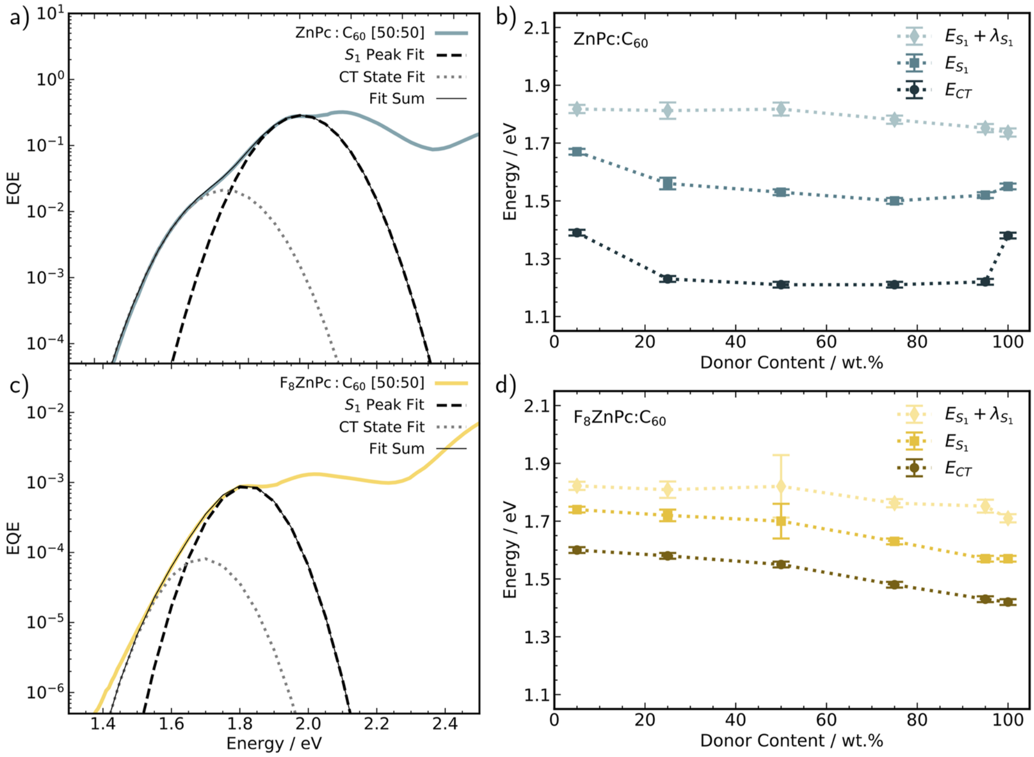

FIG. 4. (a) and (c) sEQE fitting example of (a) ZnPc:C_{60} [50:50] and (c) F_8ZnPc:C_{60} [50:50]. The singlet (S_1) peak is fit first and subtracted from the data. The remaining sEQE tail is then fit as the charge transfer (CT) state using classical Marcus theory as outlined in references.[44–46] The solid black line shows the sum of the S_1 peak and CT state fits. (b) and (d) CT state energy (E_{CT}) and donor singlet energy (E_{S_1}) as a function of (b) ZnPc:C_{60} and (d) F_8ZnPc:C_{60} mixing ratio. For comparison, the sum of E_{S_1} and the reorganization energy (λ_{S_1}) of the $S_0 \rightarrow S_1$ transition is shown. The data plotted in [(b) and (d)] are included in Table S3 in the supplementary material.

investigating energy levels of ZnPc:C_{60} blends found the same trend in E_{CT}[9] but observed a constant optical gap (and, therefore, varying ΔE_{CT}) across mixing ratios by tracking the S_1 peak position in thin film absorbance spectra.[9] While this approach risks neglecting device specific effects (e.g., modified film growth on quartz compared to full device stacks), it also does not account for the broadness (captured by the reorganization energy λ_{S_1}) of the $S_0 \rightarrow S_1$ transition and led the authors to conclude that suppressed crystallization of C_{60} with the addition of ZnPc is the main driving force for the observed performance trends. Looking only at the position of the ZnPc absorption peaks in our data [Fig. 3(a) and for clarity Fig. S7]—corresponding to $E_{S_1} + \lambda_{S_1}$ in Fig. 4(b)—would also suggest a roughly constant optical gap across ZnPc:C_{60} mixing ratios,[9] that is, significantly larger than E_{S_1} determined via reciprocity of emission and absorption of neat ZnPc thin films.[47] Our approach of fitting E_{S_1} directly from sEQE spectra significantly improves on this estimate by accounting for the blend- and device-specific intermolecular interactions, e.g., polarization effects and electrostatic interactions, that change with D–A mixing. With this, our results for E_{S_1} of intermixed ZnPc:C_{60} (1.53 ± 0.01 eV) and neat ZnPc (1.55 ± 0.01 eV) closely match previous reports.[47,48] We attribute the simultaneous shift in E_{S_1} and E_{CT} with donor content to changing polarization environments. As discussed earlier, since ZnPc aggregates with preferential orientation in a π–π stacking geometry,[8,38,49,50] morphologies and, therefore, polarization environments are expected to change for different ZnPc:C_{60} mixing ratios and aggregation regions.

In the context of quantifying voltage losses, an accurate determination of both E_{S_1} and E_{CT} is paramount for estimating ΔE_{CT} and radiative recombination (Table S4 and Fig. S12).[44,47] Comparing all materials systems, we find that the trends in E_{S_1} and E_{CT} are well reproduced by qV_{oc}^{rad}, the radiative limit of the V_{oc}, which was independently calculated via integration of the sEQE and does not rely on spectral fitting. Interestingly, radiative losses, defined as the energetic difference between E_{CT} and qV_{oc}^{rad}, are largely constant across D:C_{60} mixing ratios. The highest radiative losses (around 0.25 eV) are observed for the ZnPc blends, which is in qualitative agreement with the comparably broad absorption onset observed in the sEQE spectra [Figs. 3(a) and 3(b)]. In agreement with the results presented earlier, our sEQE analysis also reveals roughly constant ΔE_{CT} across D:C_{60} mixing ratios for the fluorinated donors. Finally, the general decrease of ΔE_{CT} with increasing donor fluorination (Table S4) matches our expectations of fluorination-induced shifts of donor energy levels toward the vacuum level.[8,22,23]

IV. DISCUSSION

We now reconcile the detailed analysis of the energy levels in the donor content series of ZnPc and F_8ZnPc with the molecular properties and trends in device performance. As discussed above, for both donor systems, the S_1–CT offset is roughly constant across all mixing ratios (Table S4 and Fig. S12). The energetic shift in S_1 (and hence the CT state) differs qualitatively between the two donor molecules. We attribute the simultaneous shift of the S_1 and CT states with donor content to changing polarization environments of the blends. The trends in V_{oc} follow the changes in the optical gap and the correspondingly lower CT state energy, which also affects non-radiative losses according to the energy gap law. For example, the S_1 and CT state energy of ZnPc is ∼150 meV lower at 50% donor content compared to the 5% donor blend. This narrowing of the optical gap already largely explains the 400 mV smaller V_{oc} in the 50% vs 5% donor blends. Benduhn *et al.* found the non-radiative voltage losses to inversely scale with CT state energy at ∼180 mV/eV, corresponding to an expected 30 mV larger non-radiative loss at 50% vs 5% donor content. The experimental difference in non-radiative voltage losses between the two blends is around 130 mV, which shows that the origins of non-radiative recombination are complex and cannot be explained by the energy gap law alone. Apart from polarization effects that lead to gap narrowing, quadrupole fields affect the energy levels with direct implications for device performance.[8,51] Since C_{60} does not have a quadrupole moment due to its symmetry, only the donors generate an electrostatic quadrupole field, with a higher number of donor molecules leading to stronger fields. Electrostatic quadrupole fields decay on shorter length scales than dipoles, and energetic shifts are most significant within a few neighboring molecules.[20] Considering that the quadrupole moments of F_xZnPc act most strongly in the π–π stacking direction,[8] the quadrupole field that an interfacial ZnPc molecule and an interfacial C_{60} molecule experience are expected to be largely the same. Consequently, donor and acceptor energy levels are shifted to the same degree, and no change in the CT state energy with donor content due to the quadrupole field is expected (the narrowing via polarization was discussed in Sec. III). This is fundamentally different for non-fullerene acceptor (NFA) systems, where both molecular species carry a non-zero quadrupole moment, and donor and acceptor molecules at the interface impose different electrostatic shifts on their neighbors. As suggested in the literature, the quadrupole moment may have a more pronounced effect on the efficiency of exciton dissociation[8,51] and thus the V_{oc}. We expect a gradual change in the IE/EA levels when transitioning from a ZnPc domain to an interfacial ZnPc molecule[51] since the quadrupole field becomes weaker closer to the interface [see Figs. 1(b) and 1(c)]. For ZnPc, $Q_D < 0$ and the gradual shift results in downward energy level bending. This means that holes experience a driving force on ZnPc to move away from the interface, thereby assisting exciton dissociation. Since the degree of energy level bending depends on the strength of the quadrupole field and hence the amount of donors present in the blend, we expect an increase in the driving force for exciton dissociation with increasing ZnPc content. This logic is analogous to a mechanism proposed for NFA blends[51,52] and is consistent with the observed trends in J_{sc} and *FF* when increasing the ZnPc content from the low donor to intermixed ZnPc:C_{60}. For F_8ZnPc, $Q_D > 0$, resulting in an upward bending of the energy levels and hence a barrier to exciton dissociation, which, following the same logic, increases with donor content. Again, this explanation is consistent with the observed J_{sc} trends for the first half of the F_8ZnPc content series. While the consideration of quadrupole effects describes the transition from low donor to intermixed D:C_{60} blends well for all systems, it does not fully rationalize the decreasing (increasing) J_{sc} when the donor content is increased beyond 50 wt. %. We hypothesize that since charge–quadrupole effects primarily influence nearest neighbors, the effect of quadrupole moments on interfacial energy levels might saturate once sufficiently large donor aggregation regions are formed. Furthermore, we highlight again that the J_{sc} is a highly convoluted quantity that not only depends on the efficiency of exciton dissociation but also on absorption (discussed earlier) and may be affected by changes in the charge collection efficiency. Given the complexity of the presented dataset, elaborate modeling linking molecular and device properties and specifically investigating the influence of quadrupole moments and percolation pathways would be beneficial. In addition, coupling our studies with other specialized techniques, e.g., mobility measurements, or time-resolved spectroscopic techniques like transient absorption spectroscopy (TAS) that can quantify efficiencies of electronic transitions, would aid in disentangling the individual contributions to the photocurrent. Nevertheless, the qualitatively opposing trends in J_{sc} between ZnPc and F_8ZnPc, and the molecules' opposing sign in quadrupole moment, provide a justified hypothesis.

V. CONCLUSIONS

In this work, we study the role of D:A mixing ratios on the energy levels and device performance of BHJs based on ZnPc or its fluorinated derivatives (F_4ZnPc, F_8ZnPc, and F_{16}ZnPc) as donors and C_{60} as the acceptor. Through J–V measurements, we find that open-circuit voltages and photocurrents are strongly dependent on D:C_{60} mixing ratios, with the ZnPc/F_4ZnPc and the F_8ZnPc/F_{16}ZnPc blends displaying similar performance trends. The device performances are rationalized via changes in molecular and blend energy levels probed by careful analysis of sEQE spectra on a linear and logarithmic scale. Our work demonstrates that fitting both singlet and CT state energies from sEQE spectra provides device-relevant information on energy level shifts and driving forces. For instance, we find that ΔE_{CT}, the energetic difference between the donor S_1 and CT states, is largely invariant to changing D:C_{60} mixing ratios in our studied material systems. With this, we rationalize trends in the V_{oc} by changing polarization effects that likely cause energy level shifts on a molecular level. Our discussion of quadrupole moments in fullerene-based blends highlights qualitatively different expected behavior in donor content series depending on the sign of the quadrupole, which is in agreement with our experimental data. Combining these insights with future studies of charge carrier dynamics could unlock a complete picture of the energetics in these blends. Our methodology of preparing D:A mixing series and carefully analyzing sEQE spectra to investigate energy levels in real BHJ devices is equally applicable to NFAs. In this context, the role of molecular quadrupole moments should be studied further to support the rational design of new molecules and donor–acceptor pairs with improved performance.

A. Experimental Methods

1. Sample fabrication

Organic solar cells were fabricated via vacuum thermal deposition using an evaporation chamber (Creaphys, EVAP300, base pressure 10^{-7} mbar). Prior to deposition, the substrates were sonicated for 10 min in a solution of 2.5% Hellmanex in DI water, followed by DI water, acetone, and isopropanol. The substrates were treated with O_2 plasma for 10 min before being loaded into the evaporation chamber. The devices were fabricated on ITO-patterned glass (Eagle XG glass, 20 Ω/sq, rms roughness < 7 Å) and through subsequent evaporation of MoO_x (3 nm, 0.05–0.1 Å/s), F_xZnPc:C_{60} (varying ratios, 50 nm, 0.4 Å/s total rate), BPhen (8 nm, 0.1–0.2 Å/s), and Al (~100 nm, 1–2 Å/s). The ITO-coated glass was purchased from Thin Film Devices TFD, Inc., USA. Optoelectronic grade C_{60} was purchased from Creaphys GmbH, Germany. ZnPc, F_4ZnPc, F_8ZnPc, F_{16}ZnPc, BPhen, and MoO_x were purchased from Luminescence Technology Corp in a sublimed form where possible. The substrates were held at room temperature during the layer-by-layer deposition of the device stacks. Post deposition, all samples were transferred into a N_2-filled glovebox without air exposure and encapsulated by a glass cover slide for further characterization. All devices reported in this work have an active area of 0.08 cm^2 as defined by the geometric overlap between the ITO and the Al electrodes.

2. Current density–voltage measurements

Current density–voltage characteristics were measured under simulated AM1.5g light using a sun simulator (Abet Technologies, Sun 2000, Class AAB) and a source meter (Keithley, 2400 Source Measure Unit). The light source was calibrated using an NREL-certified KG5 filtered silicon reference diode and set to 100 mW/cm^2 intensity with respect to the reference diode. Scans were performed in both forward and reverse directions, typically covering a range of −1 to 1.5 V and measuring in 0.02 V steps.

3. External quantum efficiency measurements

Sensitive external quantum efficiency (sEQE) measurements were performed using a custom-built setup. White light from a tungsten-halogen light source (Princeton Instruments, TS-428, 250 W) was diffracted by wavelength using a monochromator (Princeton Instruments, Spectra-Pro HRS300, Triple Grating Imaging Spectrograph). Using spectral filters (Thorlabs, edge pass, and long pass filters), stray light and higher-order diffractions were removed. The light was modulated using a chopper wheel (Stanford Research Systems, SR450, Optical Chopper) before being focused onto the device under testing. The resulting photocurrent was preamplified (Zürich Instruments, HF2TA Current Amplifier) before being read out by a Lock-In amplifier (Zürich Instruments, HF2LI Lock-In Amplifier). The sEQE spectra were calibrated using Silicon (Thorlabs, FDS100-CAL) and Indium Gallium Arsenide (Thorlabs, FGA21-CAL) photodiodes.

4. Charge transfer state analysis

Sensitive EQE spectra were fit using Marcus theory,[27,31,53] with $EQE(E) = f_{CT}/\left(E\sqrt{4\lambda_{CT}k_B T}\right) \times \exp\left(-(E_{CT} + \lambda_{CT} - E)^2/4\lambda_{CT}k_B T\right)$, where f_{CT} is an absorption pre-factor that is related to the oscillator strength, λ_{CT} describes the reorganization energy, and E_{CT} marks the charge transfer (CT) state energy. The singlet (S_1) peak was fit first using an analogous equation and subtracted from the sEQE spectrum. The remaining tail was fit as the CT state, following the methodology outlined in Refs. 44–46.

5. Voltage loss calculations

Voltage losses were calculated following the methodology outlined in Ref. 47. The singlet (S_1) and charge transfer (CT) state energies were used as reference energies. The radiative upper limit of the open-circuit voltage (V_{oc}^{rad}) was calculated assuming reciprocity between emission and absorption[47,54] and via $V_{oc}^{rad} = k_B T/q \cdot \ln\left(\int_{E_{min}}^{\infty} EQE \cdot \phi_{AM1.5g} dE / \int_{E_{min}}^{\infty} EQE \cdot \phi_{bb} dE\right)$. Here, k_B is the Boltzmann constant, T is the temperature, q is the elementary charge,

$\phi_{\text{AM1.5g}}$ is the AM1.5g light spectrum, ϕ_{bb} is the black-body spectrum, and E_{min} is minimum integration energy that was chosen such that $V_{\text{oc}}^{\text{rad}}$ saturates at the D:C$_{60}$ interface.[36,55] Radiative losses were calculated as $q\Delta V_{oc}^{rad} = E_{CT} - qV_{oc}^{rad}$, and non-radiative losses were determined via $q\Delta V_{oc}^{nr} = qV_{oc}^{rad} - V_{oc}$.

6. GIWAXS Experimental Details

Grazing incidence wide-angle x-ray scattering (GIWAXS) measurements for all except two samples were carried out at the Surface and Interface Diffraction beamline (I07) at the Diamond Light Source (DLS) using a beam energy of 20 keV (0.62 Å) and a Pilatus 2M area detector. The sample-to-detector distance was calibrated using silver behenate (AgBeh) and determined as 664.8 mm. GIWAXS measurements of the 5 and 95 wt. % F$_4$ZnPc:C$_{60}$ blends were carried out at the European Synchrotron Radiation Facility (ESRF) at BM28 (XMAS/THE UK CRG). X-ray energy of 20 keV (0.62 Å) was used, and 2D images were recorded using a Pilatus 2M detector. Air scattering was reduced by using a flight tube with Kapton windows, and the sample-to-detector distance was determined to be 421.6 mm using AgBeh. Images were converted to 2D reciprocal space using the DAWN software package with an applied polarization and solid angle correction.[56] Reciprocal space maps are shown with a logarithmic color scale to facilitate the readers' understanding of scattering features. The positions of the primary out-of-plane peaks were determined from conical slices between 2° and 5° of the out-of-plane axial orientation, which fitted as Lorentzian functions with a linearly varying background. The angular off-set is due to the missing wedge, which arises from the conversion to reciprocal space. The position of the in-plane π–π stacking peaks was determined from a rectangular region around the Yoneda band (roughly $q_z = 0.05$ Å^{-1}) and fitted in the same way. The corresponding distance in real space was found by $d = 2\pi/q$.

SUPPLEMENTARY MATERIAL

Additional data and results, including extended performance characterization, analysis of voltage losses, and microstructure measurements are given in the supplementary material.

ACKNOWLEDGMENTS

A.J. acknowledges funding from the Wolfson-Marriott Graduate Scholarship from Wolfson College, Oxford, the EPRSC Doctoral Training Accounts, and the Department of Physics at the University of Oxford. P.K., T.D., and M.R. acknowledge funding from the Global Challenges Research Fund (GCRF) through Science and Technology Facilities Council (STFC) under Grant No. ST/R002754/1: Synchrotron Techniques for African Research and Technology (START). P.K. also thanks EPSRC for funding a Postdoctoral Fellowship under Grant No. EP/V035770/1. A.E.L. thanks the EPSRC for funding through the Doctoral Training Partnership under Grant No. EP/N509711/1 as well as the STFC, ISIS Neutron, and Muon facility and studentship under Grant No. 1948713.

GIWAXS measurements were performed at the I07 beamline at the Diamond Light Source (experimental session NT26630-1) and at XMaS: The UK Materials Science Facility (BM28) at the European Synchrotron Radiation Facility (ESRF; experimental session 28-01-1274). The data can be accessed at https://data.esrf.fr/ and via https://doi.esrf.fr/10.15151/ESRF-DC-772678050. We thank Didier Wermeille (University of Liverpool), Oier Bikondoa (University of Warwick), and Jonathan Rawle (Diamond Light Source) for their invaluable help and support during the respective beamtimes.

This research was funded in part by UKRI ST/R002754/1 and EP/N509711/1. For the purpose of Open Access, the author has applied a CC BY public copyright licence to any Author Accepted Manuscript (AAM) version arising from this submission.

AUTHOR DECLARATIONS

Conflict of Interest

The authors declare no competing interest.

Author Contributions

A.J., P.K., and M.R. designed and coordinated the project. A.J. carried out all sample fabrication and device measurements. A.E.L. and T.D. performed the GIWAXS measurements and analysis. All authors contributed to the analysis and manuscript writing.

Anna Jungbluth: Conceptualization (equal); Data curation (lead); Formal analysis (equal); Investigation (lead); Methodology (lead); Project administration (equal); Software (lead); Validation (equal); Visualization (lead); Writing – original draft (lead); Writing – review & editing (equal). **Pascal Kaienburg**: Conceptualization (equal); Data curation (supporting); Formal analysis (equal); Investigation (supporting); Methodology (supporting); Project administration (equal); Supervision (supporting); Validation (equal); Visualization (supporting); Writing – review & editing (equal). **Andreas E. Lauritzen**: Data curation (supporting); Formal analysis (supporting); Investigation (supporting); Writing – review & editing (supporting). **Thomas Derrien**: Data curation (supporting); Formal analysis (supporting); Investigation (supporting); Writing – review & editing (supporting). **Moritz Riede**: Conceptualization (equal); Formal analysis (supporting); Funding acquisition (lead); Investigation (supporting); Methodology (supporting); Project administration (equal); Supervision (lead); Validation (equal); Visualization (supporting); Writing – review & editing (equal).

DATA AVAILABILITY

The data that support the findings of this study are available from the corresponding author upon reasonable request.

REFERENCES

[1] C. M. Wolff, P. Caprioglio, M. Stolterfoht, and D. Neher, "Nonradiative recombination in perovskite solar cells: The role of interfaces," Adv. Mater. **31**(52), 1902762 (2019).

[2] J. Cornil *et al.*, "Exploring the energy landscape of the charge transport levels in organic semiconductors at the molecular scale," Acc. Chem. Res. **46**(2), 434–443 (2013).

[3] K. Vandewal, "Interfacial charge transfer states in condensed phase systems," Annu. Rev. Phys. Chem. **67**, 113 (2016).

[4] J. Bertrandie *et al.*, "The energy level conundrum of organic semiconductors in solar cells," Adv. Mater. **34**(35), 2202575 (2022).

[5] M. C. Scharber *et al.*, "Design rules for donors in bulk-heterojunction solar cells—Towards 10% energy-conversion efficiency," Adv. Mater. **18**(6), 789–794 (2006).

[6] P. I. Djurovich, E. I. Mayo, S. R. Forrest, and M. E. Thompson, "Measurement of the lowest unoccupied molecular orbital energies of molecular organic semiconductors," Org. Electron. **10**(3), 515–520 (2009).

[7] L. Leonat, G. Sbârcea, and I. V. Brânzoi, "Cyclic voltammetry for energy levels estimation of organic materials," U.P.B. Sci. Bull., Ser. B **75**(3), 111 (2013).

[8] M. Schwarze *et al.*, "Impact of molecular quadrupole moments on the energy levels at organic heterojunctions," Nat. Commun. **10**(1), 2466 (2019).

[9] M. L. Tietze *et al.*, "Correlation of open-circuit voltage and energy levels in zinc-phthalocyanine: C_{60} bulk heterojunction solar cells with varied mixing ratio," Phys. Rev. B **88**(8), 085119 (2013).

[10] G. D'Avino *et al.*, "Electrostatic phenomena in organic semiconductors: Fundamentals and implications for photovoltaics," J. Phys.: Condens. Matter **28**(43), 433002 (2016).

[11] C. Poelking and D. Andrienko, "Long-range embedding of molecular ions and excitations in a polarizable molecular environment," J. Chem. Theory Comput. **12**(9), 4516–4523 (2016).

[12] N. Sato, K. Seki, and H. Inokuchi, "Polarization energies of organic solids determined by ultraviolet photoelectron spectroscopy," J. Chem. Soc., Faraday Trans. 2 **77**(9), 1621–1633 (1981).

[13] N. Sato, H. Inokuchi, and E. A. Silinsh, "Reevaluation of electronic polarization energies in organic molecular crystals," Chem. Phys. **115**(2), 269–277 (1987).

[14] K. R. Graham *et al.*, "The roles of structural order and intermolecular interactions in determining ionization energies and charge-transfer state energies in organic semiconductors," Adv. Energy Mater. **6**(22), 1601211 (2016).

[15] S. Duhm *et al.*, "Orientation-dependent ionization energies and interface dipoles in ordered molecular assemblies," Nat. Mater. **7**(4), 326–332 (2008).

[16] F. Piersimoni *et al.*, "Influence of fullerene ordering on the energy of the charge-transfer state and open-circuit voltage in polymer:fullerene solar cells," J. Phys. Chem. C **115**(21), 10873–10880 (2011).

[17] F. C. Jamieson, E. B. Domingo, T. McCarthy-Ward, M. Heeney, N. Stingelin, and J. R. Durrant, "Fullerenecrystallisation as a key driver of charge separation in polymer/fullerene bulk heterojunction solar cells," Chem. Sci. **3**(2), 485–492 (2012).

[18] D. Veldman *et al.*, "Compositional and electric field dependence of the dissociation of charge transfer excitons in alternating polyfluorene copolymer/fullerene blends," J. Am. Chem. Soc. **130**(24), 7721–7735 (2008).

[19] C. Poelking *et al.*, "Impact of mesoscale order on open-circuit voltage in organic solar cells," Nat. Mater. **14**(4), 434–439 (2015).

[20] A. Privitera, G. Londi, M. Riede, G. D'Avino, and D. Beljonne, "Molecular quadrupole moments promote ground-state charge generation in doped organic semiconductors," Adv. Funct. Mater. **30**(45), 2004600 (2020).

[21] R. Warren *et al.*, "Controlling energy levels and Fermi level en route to fully tailored energetics in organic semiconductors," Nat. Commun. **10**(1), 5538 (2019).

[22] M. Brendel *et al.*, "The effect of gradual fluorination on the properties of FnZnPc thin films and FnZnPc/C_{60} bilayer photovoltaic cells," Adv. Funct. Mater. **25**(10), 1565–1573 (2015).

[23] J. Meiss *et al.*, "Fluorinated zinc phthalocyanine as donor for efficient vacuum-deposited organic solar cells," Adv. Funct. Mater. **22**(2), 405–414 (2012).

[24] K. Vandewal *et al.*, "Fourier-Transform Photocurrent Spectroscopy for a fast and highly sensitive spectral characterization of organic and hybrid solar cells," Thin Solid Films **516**(20), 7135–7138 (2008).

[25] K. Vandewal *et al.*, "The relation between open-circuit voltage and the onset of photocurrent generation by charge-transfer absorption in polymer: Fullerene bulk heterojunction solar cells," Adv. Funct. Mater. **18**(14), 2064–2070 (2008).

[26] R. A. Marcus, "Relation between charge transfer absorption and fluorescence spectra and the inverted region," J. Phys. Chem. **93**, 3078 (1989).

[27] R. A. Marcus, "Electron transfer reactions in chemistry. Theory and experiment," Rev. Mod. Phys. **65**, 599 (1993).

[28] R. A. Marcus, "On the theory of oxidation-reduction reactions involving electron transfer. I," J. Chem. Phys. **24**, 966 (1956).

[29] R. A. Marcus, "On the theory of oxidation-reduction reactions involving electron transfer. II. Applications to data on the rates of isotopic exchange reactions*," J. Chem. Phys. **26**, 867 (1957).

[30] K. Vandewal, K. Tvingstedt, A. Gadisa, O. Inganäs, and J. v. Manca, "On the origin of the open-circuit voltage of polymer-fullerene solar cells," Nat. Mater. **8**(11), 904–909 (2009).

[31] K. Vandewal, K. Tvingstedt, A. Gadisa, O. Inganä, and J. v. Manca, "Relating the open-circuit voltage to interface molecular properties of donor: Acceptor bulk heterojunction solar cells," Phys. Rev. B **81**, 125204 (2010).

[32] A. Jungbluth, E. Cho, A. Privitera *et al.*, "Limiting factors for charge generation in low-offset fullerene-based organic solar cells," Research Square preprint: 10.21203/rs.3.rs-2150858/v1 (2022).

[33] I. Ramirez *et al.*, "The role of spin in the degradation of organic photovoltaics," Nat. Commun. **12**(1), 471 (2021).

[34] G. J. Moore *et al.*, "Ultrafast charge dynamics in dilute-donor versus highly intermixed TAPC:C_{60} organic solar cell blends," J. Phys. Chem. Lett. **11**(14), 5610–5617 (2020).

[35] T. Lee, A. Sanzogni, N. Zhangzhou, P. L. Burn, and A. E. Mark, "Morphology of a bulk heterojunction photovoltaic cell with low donor concentration," ACS Appl. Mater. Interfaces **10**(38), 32413–32419 (2018).

[36] M. Zhang, H. Wang, H. Tian, Y. Geng, and C. W. Tang, "Bulk heterojunction photovoltaic cells with low donor concentration," Adv. Mater. **23**(42), 4960–4964 (2011).

[37] W. Tress, "Open circuit voltage and IV curve shape of ZnPc:C_{60} solar cells with varied mixing ratio and hole transport layer," Proc. SPIE **1**(1), 011114 (2011).

[38] C. Schünemann, C. Elschner, A. A. Levin, M. Levichkova, K. Leo, and M. Riede, "Zinc phthalocyanine—Influence of substrate temperature, film thickness, and kind of substrate on the morphology," Thin Solid Films **519**(11), 3939–3945 (2011).

[39] P. Simon, B. Maennig, and H. Lichte, "Conventional electron microscopy and electron holography of organic solar cells," Adv. Funct. Mater. **14**(7), 669–676 (2004).

[40] T. Mönch *et al.*, "Experimental and theoretical study of phase separation in ZnPc:C_{60} blends," Org. Electron. **27**, 183–191 (2015).

[41] W. Schindler, M. Wollgarten, and K. Fostiropoulos, "Revealing nanoscale phase separation in small-molecule photovoltaic blends by plasmonic contrast in the TEM," Org. Electron. **13**(6), 1100–1104 (2012).

[42] S. Pfuetzner *et al.*, "The influence of substrate heating on morphology and layer growth in C_{60}:ZnPc bulk heterojunction solar cells," Org. Electron. **12**(3), 435–441 (2011).

[43] A. Melianas *et al.*, "Charge transport in pure and mixed phases in organic solar cells," Adv. Energy Mater. **7**(20), 1700888 (2017).

[44] A. Jungbluth, P. Kaienburg, and M. Riede, "Charge transfer state characterization and voltage losses of organic solar cells," J. Phys.: Mater. **5**(2), 024002 (2022).

[45] V. C. Nikolis *et al.*, "Field effect versus driving force: Charge generation in small-molecule organic solar cells," Adv. Energy Mater. **10**(47), 2002124 (2020).

[46] T.-y. Li *et al.*, "Boron dipyrromethene (BODIPY) with *meso*-perfluorinated alkyl substituents as near infrared donors in organic solar cells," J. Mater. Chem. A **6**(38), 18583–18591 (2018).

[47] K. Vandewal, J. Benduhn, and V. C. Nikolis, "How to determine optical gaps and voltage losses in organic photovoltaic materials," Sustainable Energy Fuels **2**(3), 538–544 (2018).

[48] J. Benduhn *et al.*, "Impact of triplet excited states on the open-circuit voltage of organic solar cells," Adv. Energy Mater. **8**(21), 1800451 (2018).

[49] C. Schünemann *et al.*, "Phase separation analysis of bulk heterojunctions in small-molecule organic solar cells using zinc-phthalocyanine and C_{60}," Phys. Rev. B **85**(24), 245314 (2012).

[50] C. Schünemann, D. Wynands, K.-J. Eichhorn, M. Stamm, K. Leo, and M. Riede, "Evaluation and control of the orientation of small molecules for strongly absorbing organic thin films," J. Phys. Chem. C **117**(22), 11600–11609 (2013).

[51] S. Karuthedath *et al.*, "Intrinsic efficiency limits in low-bandgap non-fullerene acceptor organic solar cells," Nat. Mater. **20**(3), 378–384 (2021).

[52] Y. Fu *et al.*, "Molecular orientation-dependent energetic shifts in solution-processed non-fullerene acceptors and their impact on organic photovoltaic performance," Nat. Commun. **14**(1), 1870 (2023).

[53] R. A. Marcus, "Chemical and electrochemical electron-transfer theory," Annu. Rev. Phys. Chem. **15**, 155 (1964).

[54] U. Rau, "Reciprocity relation between photovoltaic quantum efficiency and electroluminescent emission of solar cells," Phys. Rev. B **76**(8), 085303 (2007).

[55] P. Kaienburg, A. Jungbluth, I. Habib, S. V. Kesava, M. Nyman, and M. K. Riede, "Assessing the photovoltaic quality of vacuum-thermal evaporated organic semiconductor blends," Adv. Mater. **34**(22), 2107584 (2022).

[56] J. Filik *et al.*, "Processing two-dimensional X-ray diffraction and small-angle scattering data in DAWN 2," J. Appl. Crystallogr. **50**(3), 959–966 (2017).

[57] N. Sato, K. Seki, and H. Inokuchi, "Polarization energies of organic solids determined by ultraviolet photoelectron spectroscopy," J. Chem. Soc., Faraday Trans. 2 **77**, 1621 (1981).

[58] W. Tress, *Organic Solar Cells* (Springer International Publishing, Cham, 2014), Vol. 208.

[59] J.-L. Bredas, "Mind the gap!," Mater. Horiz. **1**(1), 17–19 (2014).